

# Liquid micro-lens array activated by selective electrowetting on lithium niobate substrates

S. Grilli, L. Miccio, V. Vespini, A. Finizio, S. De Nicola, and Pietro Ferraro

*Istituto Nazionale di Ottica Applicata (CNR-INOA) & Istituto di Cibernetica del CNR "E. Caianiello",  
Via Campi Flegrei 34 – 80078 Pozzuoli (NA), Italy  
[simonetta.grilli@inoa.it](mailto:simonetta.grilli@inoa.it), [lisa.miccio@inoa.it](mailto:lisa.miccio@inoa.it), [pietro.ferraro@inoa.it](mailto:pietro.ferraro@inoa.it)*

**Abstract:** Lens effect was obtained in an open microfluidic system by using a thin layer of liquid on a polar electric crystal like LiNbO<sub>3</sub>. An array of liquid micro-lenses was generated by electrowetting effect in pyroelectric periodically poled crystals. Compared to conventional electrowetting devices, the pyroelectric effect allowed to have an electrode-less and circuit-less configuration. An interferometric technique was used to characterize the curvature of the micro-lenses and the corresponding results are presented and discussed. The preliminary results concerning the imaging capability of the micro-lens array are also reported.

©2008 Optical Society of America

**OCIS codes:** (010.1080) adaptive optics; (220.2560) focus, (220.3630) lenses; liquid lens; optofluidic; (090.0090) holography.

---

## References and links

1. P. Ferraro, "What breaks the shadow of the tube?" *The Physics Teacher* **36**, 542-543 (1998).
2. B. Berge and J. Peseux, "Variable focal lens controlled by an external voltage: an application of electrowetting," *Eur. Phys. J. E* **3**, 159-163 (2000).
3. D. Grahnan-Rowen, "Liquid lenses make a splash," *Nat. Photonics* **Volume sample**, 2-4 (2006).
4. G. Beni and M. A. Tenan, "Dynamics of electrowetting displays," *J. Appl. Phys.* **52**, 6011-6015 (1981).
5. R. Hayes and D. J. Feenstra, "Video-Speed electronic paper based on electrowetting," *Nature* **425**, 383-385 (2003).
6. S. Kuiper and B. H. W. Hendriks, "Variable-focus liquid lens for miniature cameras," *Appl. Phys. Lett.* **85**, 1128-1130 (2004).
7. L. Dong, A. K. Argawal, D. J. Beebe, and H. Jiang, "Adaptive liquid microlenses activated by stimuli-responsive hydrogels," *Nature* **442**, 551-554 (2006).
8. C. C. Cheng and J. A. Yeh, "Dielectrically actuated liquid lens," *Opt. Express* **15**, 7140-7145 (2007).
9. D. Psaltis, S. R. Quache, and C. Yang, "Developing optofluidic technology through the fusion of microfluidics and optics," *Nature* **442**, 381-386 (2006).
10. F. Mugele and S. Herminghaus, "Electrostatic stabilization of fluid microstructures," *Appl. Phys. Lett.* **81**, 2303-2305 (2002).
11. T. Beerling, "Liquid metal switch employing an electrically isolated control element," US Patent N. 7,053,323 (2006).
12. P. M. Moran, S. Dharmatilleke, A. H. Khaw, K. W. Tan, M. L. Chan, and I. Rodriguez, "Fluidic lenses with variable focal length," *Appl. Phys. Lett.* **88**, 041120-3 (2006).
13. H. Ren, D. Fox, P. A. Anderson, B. Wu, S.-T. Wu, "Tunable-focus liquid lens controlled using a servo motor," *Opt. Express* **14**, 8031-8036 (2006).
14. B. S. Gallardo, V. K. Gupta, F. D. Eagerton, L. I. Jong, V. S. Craig, R. R. Shah, and N. L. Abbott, "Electrochemical principles for active control of liquids on submillimeter scales," *Sci.* **283**, 57-60 (1999).
15. E. Colgate and H. Matsumoto, "An investigation of electrowetting-based micro actuation," *J. Vac. Sci. Technol. A* **8**, 3625-3633 (1990).
16. A. Sharma and R. Khanna, "Pattern formation in unstable thin liquid films," *Phys. Rev. Lett.* **81**, 3463-3466 (1998).
17. D. E. Kataoka and S. M. Troian, "Patterning liquid flow on the microscopic scale," *Nature* **402**, 794-797 (1999).
18. R. Seemann, M. Brinkmann, E. J. Kramer, F. F. Lange, and R. Lipowsky, "Wetting morphologies at microstructured surfaces," *PNAS* **102**, 1848-1852 (2005).

19. H. Moon, S. K. Cho, R. L. Garrell, and C.-J. Kim, "Low voltage electrowetting-on-dielectric," *J. Appl. Phys.* **92**, 4080-4087 (2002).
20. D. Aronov, G. Rosenman, A. Karlov, and A. Shashkin, "Wettability patterning of hydroxyapatite nanobioceramics induced by surface potential modification," *Appl. Phys. Lett.* **88**, 163902-3 (2006).
21. D. B. Wang, R. Szoszkiewicz, M. Lucas, E. Riedo, T. Okada, S. C. Jones, S. R. Marder, J. Lee, and W. P. King, "Local wettability modification by thermochemical nanolithography with write-read-overwrite capability," *Appl. Phys. Lett.* **91**, 243104-3 (2007).
22. M. W. J. Prinse, W. J. J. Welters, and J. W. Weekamp, "Fluid control in multichannel structures by electrocapillary pressure," *Sci.* **291**, 277-280 (2001).
23. C. W. Monroe, L. I. Daikhin, M. Urbakh, and A. A. Kornyshev, "Electrowetting with electrolytes," *Phys. Rev. Lett.* **97**, 136102-4 (2006).
24. P. Lazar and H. Riegler, "Reversible self propelled droplet movement: a new driving mechanism," *Phys. Rev. Lett.* **95**, 136103-4 (2005).
25. F. Mugele and J.-C. Baret, "Electrowetting: from basics to applications," *J. Phys. Condens. Matter* **17**, R705-R774 (2005).
26. E. L. Wooten, K. M. Kissa, A. Yi-Yan, E. J. Murphy, D. A. Lafaw, P. F. Hallemeier, D. Maack, D. V. Attanasio, D. J. Fritz, G. J. McBrien, and D. E. Bossi, "A Review of Lithium Niobate Modulators for Fiber-Optic Communications Systems," *IEEE J. Sel. Top. Quantum Electron.* **6**, 69-82 (2000).
27. R. L. Byer, "Nonlinear Optics and Solid-State Lasers:2000," *IEEE J. Sel. Top. Quantum Electron.* **6**, 911-930 (2000).
28. F. Laurell, M. G. Roelofs, W. Bindloss, H. Hsiung, A. Suna, and J. D. Bierlein, "Detection of ferroelectric domain reversal in KTP waveguides," *J. Appl. Phys.* **71**, 4664-4670 (1992).
29. B. Sun and J. Heikenfeld "Observation and optical implications of oil dewetting patterns in electrowetting displays" *J. Micromech. Microeng.* **18**, 025027 (2008)
30. C. H. Bulmer, W. K. Burns, and S. C. Hiser, "Pyroelectric effects in LiNbO<sub>3</sub> channel waveguide devices," *Appl. Phys. Lett.* **48**, 1036-1038 (1986).
31. M. Yamada, N. Nada, M. Saitoh, and K. Watanabe, "First-order quasi-phase matched LiNbO<sub>3</sub> waveguide periodically poled by applying an external field for efficient blue second-harmonic generation," *Appl. Phys. Lett.* **62**, 435-436 (1993).
32. S. Grilli, M. Paturzo, L. Miccio, and P. Ferraro, "*In situ* investigation of periodic poling in congruent LiNbO<sub>3</sub> by quantitative interference microscopy," *Meas. Sci. Technol.* (in press).
33. K. Nassau, H. J. Levinstein, and G. M. Loiacono, "The domain structure and etching of ferroelectric lithium niobate," *Appl. Phys. Lett.* **6**, 228-229 (1965).
34. S. Grilli, P. Ferraro, P. De Natale, B. Tiribilli, and M. Vassalli, "Surface nanoscale periodic structures in congruent lithium niobate by domain reversal patterning and differential etching," *Appl. Phys. Lett.* **87**, 233106-3 (2005).
35. V. Gopalan and T. E. Mitchell, "*In situ* video observation of 180° domain switching in LiTaO<sub>3</sub> by electro-optic imaging microscopy," *J. Appl. Phys.* **85**, 2304-2311 (1999).
36. R. S. Weis and T. K. Gaylord, "Lithium Niobate: Summary of Physical Properties and Crystal Structure," *Appl. Phys. A* **37**, 191-203 (1985).
37. E. M. Bourim, C.-W. Moon, S.-W. Lee, and I. K. Yoo, "Investigation of pyroelectric electron emission from monodomain lithium niobate single crystals," *Phys. B* **383**, 171-182 (2006).
38. B. Rosenblum, P. Bräunlich, and J. P. Carrico, "Thermally stimulated field emission from pyroelectric LiNbO<sub>3</sub>," *Appl. Phys. Lett.* **25**, 17-19 (1974).
39. G. Rosenman, D. Shur, Y. E. Krasik, and A. Dunaevsky, "Electron emission from ferroelectrics," *J. Appl. Phys.* **88**, 6109-6161 (2000).
40. F. Beunis, F. Strubbe, M. Marescaux, K. Neyts, and A. R. M. Verschueren, "Diffuse double layer charging in nonpolar liquids," *Appl. Phys. Lett.* **91**, 182911-3 (2007).
41. M. G. Lippmann, *Ann. Chim. Phys.* **5**, 494 (1875).
42. P. Ferraro, S. De Nicola, and G. Coppola, "Digital holography: recent advancements and prospective improvements for applications in microscopy" in *Optical Imaging Sensors and Systems for Homeland Security Applications*, vol. 2 of *Advanced Sciences and Technologies for Security Applications* series B. Javidi ed., (Springer, 2005), pp. 47-84.

## 1. Introduction

The liquid lens effect is well known and several examples can be found in nature. Lensing lighting intensity patterns can be observed on the bottom of a swimming pool or caused by the curvature of the water induced by the surface tension [1]. The most popular and well-established approach to obtain liquid lenses is based on the electrowetting effect [2]. The electrode-based liquid lenses usually consist of two immiscible liquids manipulated into

special cases made of hydrophobic coatings and electrodes. The applied voltage changes the equilibrium among the various forces acting between liquid-to-liquid and solid-liquid interfaces causing a reshaping and re-arrangement of the liquid meniscus. The change of curvature, in modulus and sign, has direct effect on the refraction of through-transmitted light, thus allowing to switch between a converging and a diverging lens with flexible focal lengths [3-9]. Single or multiple wells, covered with an hydrophobic coating, are also used as electrodes. A sessile liquid drop free standing on a flat electrode surface can be manipulated by a second needle-like electrode immersed into the drop [10]. Another possible configuration consists of a liquid drop between two plane parallel electrodes, useful for the fabrication of complex optical switches [4,11]. The pressure-driven liquid lenses make use of a small liquid reservoir having flexible and transparent membranes. The lens shape, and thus the focal power of the microfluidic lens, can be changed by varying the hydrostatic pressure of the liquid volume [12,13]. The development of all of these liquid lens configurations has benefited from the strong progress achieved into the field of microfluidics during the recent past years. Research activities on electrowetting, or more in general studies on wettability and dewettability [14-25] of surfaces, have been performed since long time not necessarily related to the field of optics, but rather with the aim at patterning liquids on surfaces. An interesting overview about the scope, the methods and the results is provided by ref. [25] where open microfluidic systems are considered.

This paper deals with the liquid lens effect obtainable by pyroelectrically activated electrowetting effect onto lithium niobate (LN) substrates. As described above, the operation of conventional electrowetting-based microfluidic devices demands more or less complex electrode geometries to actuate a liquid lens, thus requiring special technological steps and materials for the fabrication. The possibility to functionalize a specific and appropriate material to get a microfluidic lens array on a single chip is foreseen in this paper. This vision could lead to the realization in future of an optofluidic lens array on a microscopic scale.

## 2. Observation of lens effect

LN crystal substrates were used in this work to demonstrate the possibility to get a liquid lens array with variable curvature and focal length. LN is a very well known ferroelectric material widely used as a key element in optical modulators for fibre optic telecommunications [26] and in non-linear optic devices [27]. To the best of our knowledge, the possibility to change the topography of a thin liquid film onto a microengineered LN substrate by the pyroelectric effect [28,30] was observed for the first time in this work. The topography variation allows to build-up a liquid microlens array activated by temperature gradients on the LN surface. The resulting structure can be considered as an open microfluidic system [18] exhibiting lens effect. In the past, regular arrays of liquid lenses have been observed by means of the electrowetting effect based on the spinodal dewetting theory [29].

The spontaneous polarization of LN crystals can be reversed by the electric field poling process [31,32], thus enabling the fabrication of periodically poled LN (PPLN) crystals. An external voltage exceeding the coercive field of the material (around 21 kV/mm) is necessary to reverse the ferroelectric domains and the inversion selectivity is usually ensured by an appropriate resist pattern generated by photolithography [32]. Figure 1 shows the optical microscope image of two PPLN samples fabricated by the electric field poling and used for the lens effect experiments investigated here. The samples consist of a square array of bulk reversed domains with a period around 200  $\mu\text{m}$  along both  $x$  and  $y$  direction. In fact, the lens array effect was first investigated and presented here in case of a relatively simple geometry as the square array, in order to demonstrate the reliability and feasibility of the pyroelectrically driven liquid lens effect. Anyway, more complex geometries, such as hexagonal or circular arrays, could be used for further investigations, by simply providing the appropriate photolithographic mask for the pattern generation. The two samples in Fig. 1 differ only for the geometry of the resist openings (see Ref. [32] for details) and both of them were used for

the same lens effect experiments, in order to test the reliability of the technique. The samples were not etched, contrary to the conventional procedure used to visualize the domain pattern [33,34]. In fact, the reversed domains are visible thanks to the contrast enhancement provided by the appropriate aperture of the condenser diaphragm, thus improving the diffraction image of the domain walls related to the electro-optic effect induced by the so called internal field [35] arising after the electric field poling. The PPLN sample was mounted onto a digitally controlled hot-plate to ensure a reliable control of the substrate temperature during the experiments. The liquid used in this work was a carboxylic acid (pentanoic acid -  $C_5H_{10}O_2$ ) in the form of an oily substance. The values of the dielectric constant and of the refractive index are 2.66 and 1.407-1.41, respectively. The PPLN sample was coated with a thin film of this oil (oil thickness is about  $200\mu m$ ) and subject first to an heating process up to  $100^\circ C$  at a rate of around  $20^\circ C$  per minute, and then let cooling down to room temperature.

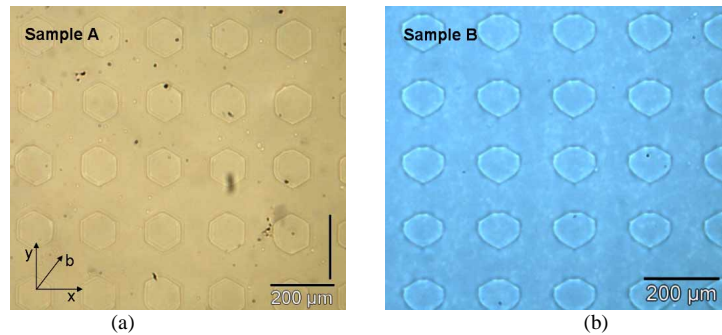


Fig. 1. Optical microscope image of two PPLN samples with a square array of reversed domains. The period of the structures is around  $200\mu m$ . A different mask was used for the two samples.

Figures 2(a)-2(b) show the optical microscope movies of the oil coated sample A under heating and cooling process, respectively.

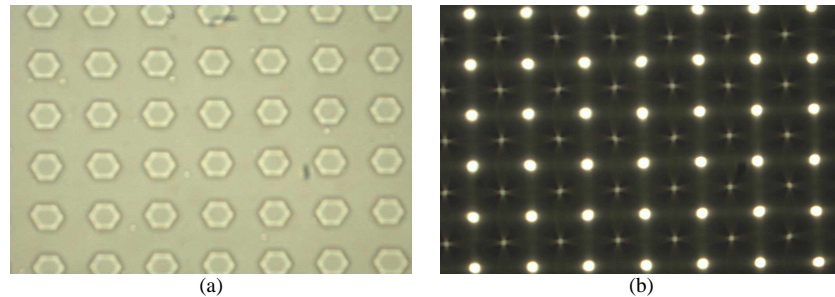


Fig. 2. Optical microscope movies of the oil coated sample A (a) under heating [3.3MB] and (b) cooling process [4.4MB].

The heating process was performed by increasing the temperature from  $40^\circ C$  up to  $100^\circ C$ . The cooling was achieved by letting the temperature to decrease from  $100^\circ C$  down to  $40^\circ C$ , thus with an approximate rate of  $12^\circ C/min$ . The whole process took about 5 minutes and the liquid lens array kept stable topography for about 30 minutes at  $40^\circ C$ , after its formation. The evolution of the oil film topography is clearly visible in both movies and, in particular, the lens effect is more pronounced in case of the cooling process. This is reasonably due to the different nature of the surface charges generating the electric potential modulation on the substrate, as discussed in the following section. The liquid microlenses were formed in

correspondence of the hexagonal domains and thus with a lateral dimension of about 100  $\mu\text{m}$ . Practical limitations to the fabrication of smaller lenses is not expected because reversed domains with lateral dimensions down to tens of micron can be reliably obtained in LN substrates. Anyway, the performance of the smaller lenses would be dramatically affected by the consequent enhancement of the diffraction effects due to the fact that the lens aperture became comparable with wavelength. It is important to note that the response of the liquid lens array was quite fast. In fact, the lens array was formed about 1 s after the temperature started to decrease.

Moreover, the lens formation followed faithfully the domain grating, thus exhibiting perfect homogeneity over the whole patterned region. In principle, liquid microlens arrays would be possible with areas as large as desirable depending basically on the area obtainable by the lithographic process used for the domain inversion process. In fact, Fig. 2 shows clearly the degree of uniformity obtainable by the technique, with a field of view including 42 lens elements corresponding to an area of about  $(1.4 \times 1.2) \text{ mm}^2$ . The limited field of view corresponding to the chosen magnification prevented to report larger view images.

### 3. Interpretation of the phenomenon

It is well known that LN is a rhombohedral crystal belonging to the point group 3m at room temperature [36]. The lack of inversion symmetry induces different effects including the pyroelectricity. This is the manifestation of the spontaneous polarization change  $\Delta P_s$  following to a temperature variation  $\Delta T$ , according to  $\Delta P_i = p_i \Delta T$ , where  $\Delta P_i$  is the coefficient of the polarization vector and  $p_i$  is the pyroelectric coefficient. At equilibrium, all  $P_s$  in the crystal are fully screened by the external screening charge and no electric field exists [37]. The change of the polarization, occurring with temperature variation, perturbs such equilibrium, causing a lack or excess of surface screening charge. Consequently, an electrostatic state appears and generates a high electric field at the crystal surface [38,39]. Figures 3(a)-3(b) show the schematic view of the PPLN sample cross section with the charge distribution occurring at the equilibrium state and in case of heating/cooling treatment, respectively. The arrows indicate the orientation of the ferroelectric domains.

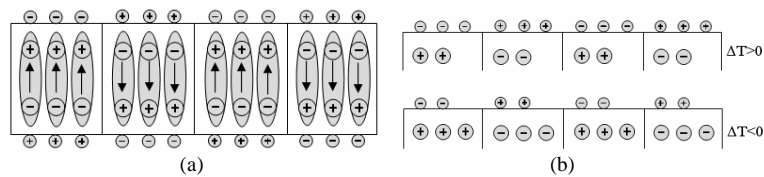


Fig. 3. Schematic view of the PPLN sample cross section with the charge distribution exhibited (a) at the equilibrium state; (b) in case of heating (top) and (bottom) cooling process.

According to the pyroelectric effect [37] the heating process makes the polarization magnitude to decrease, thus leaving surface screening charges uncompensated (see Fig. 3(b) top). These generate a net electric charge distribution depending on the inverted domain structure, with positive and negative sign onto the reversed and un-reversed domain regions, respectively. The screening charges in excess, continuously produced during the heating process, are no more attracted by the polarization charge and consequently are free to diffuse into the oil film. Conversely, the cooling process makes the polarization magnitude to increase, thus generating an electric charge onto the crystal surface (see Fig. 3(b) bottom) and giving place to the so called “double charge layer” at the solid-oil interface [15,39]. In fact, the uncompensated polarization charge tends to interact with the dipole molecules in the oil, thus redistributing them in proximity of the solid surface. Therefore, the more pronounced lens effect observed in case of cooling (see Fig. 2(b)) is due to the electrostatic action of the uncompensated polarization charge which is more intense compared to that of the screening charges during

heating. The lens-like array topography exhibited by the oil film can be considered as the result of the equilibrium condition between the surface tensions and the electric forces related to the charge redistribution on the substrate. In the general case of a sessile droplet, the surface tensions at the solid-liquid  $\gamma_{sl}$ , solid-gas  $\gamma_{sg}$  and liquid-gas  $\gamma_{lg}$  interfaces are described by the one-dimensional Young equation:

$$\gamma_{sl} + \gamma_{lg} \cos\vartheta = \gamma_{sg} \quad (1)$$

where  $\vartheta$  corresponds to the contact angle of the droplet. The charges at the solid-liquid interface reduce the surface tension according to the Lippman equation [41]:

$$\gamma_{sl}(V) = \gamma_{sl0} - \frac{1}{2} cV^2 \quad (2)$$

where  $\gamma_{sl0}$  corresponds to zero charge condition and  $c$  is the capacitance per unit area assuming that the charge layer can be modelled as a symmetric Helmholtz capacitor [15]. It is important to note that in the present work the surface was not a metal and the liquid was not an electrolyte, as basically assumed by the double charge model [15,40]. However, a similar model can be as well invoked even in case of dielectric surfaces [25]. Therefore, in the case investigated here, the presence of the net electric charge underneath the crystal surface (see bottom drawing in Fig. 2(b)), generated pyroelectrically, lowers the surface tension due to the repulsion between like charges that make the work for expanding the surface area [39]. The air-liquid interface exhibits a waviness profile to minimize the energy of the whole system. Simulations of the electric potential distribution, generated pyroelectrically, were performed by a finite element based calculation and Fig. 4(a) shows the result. The plot refers to a section along a diagonal direction (direction  $b$  in Fig. 1).

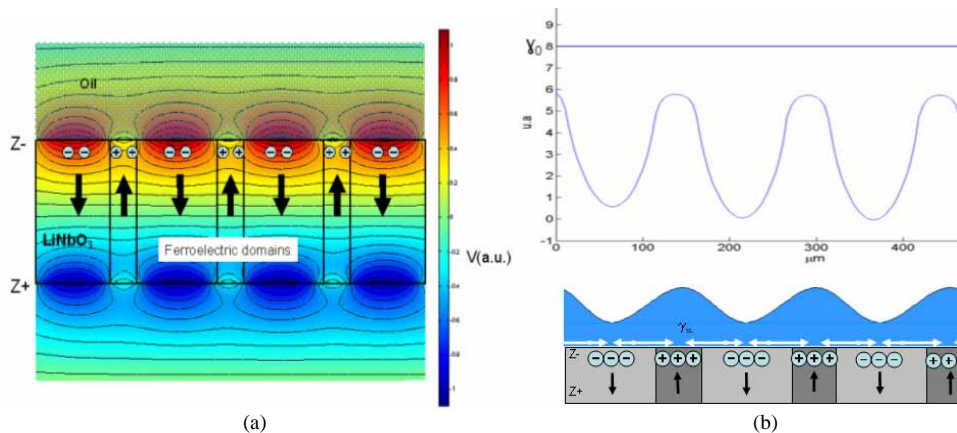


Fig. 4. (a). Schematic view of the sample cross section with the simulated electric potential distribution generated pyroelectrically; (b) (top) surface tension profile and (bottom) the schematic view of the corresponding oil film topography. The black arrows indicate the orientation of the spontaneous polarization.

The simulation clearly shows that the electric potential is modulated according to the domain structure, thus exhibiting minimum value in correspondence of the hexagon centres. The surface tension profile was then calculated by using Eq. (2) and the corresponding behaviour, in accordance with the experimental results, is shown in Fig. 4(b). In fact, the solid-liquid interface tension appears to be modulated according to the electric potential. It is important to consider that the number of charges between two consecutive hexagons is higher along the  $b$  direction compared to the horizontal or vertical direction. Therefore, the work done by the charges along the  $b$  direction produces a stronger hydrostatic pressure towards hexagon centres, thus leading to the formation of liquid micro lenses in correspondence of the hexagons.

#### 4. Characterization of the liquid micro-lens array by an interferometric method

The microfluidic system was observed and investigated during the cooling process by an interferometric apparatus based on Digital Holography [42]. The schematic view of the optical set-up used for the acquisition of the images is shown in Fig. 5.

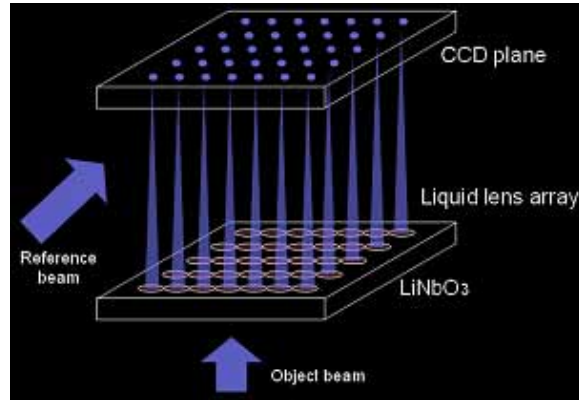


Fig. 5. Schematic view of the interferometric configuration. A sequence of digital holograms have been recorded on the CCD plane. An additional lens was used (not shown in the figure to simplify the drawing) and located between the lens-array and the CCD plane to magnify the image of the lens array.

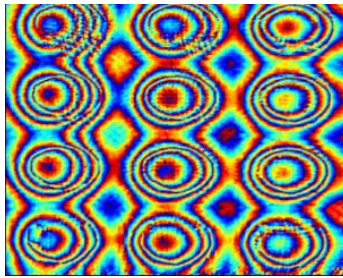


Fig. 6. Movie [4MB] of the evolving two-dimensional distribution of the wrapped phase map, modulo  $2\pi$ , corresponding to  $3 \times 4$  lens elements on the incoming collimated beam, during cooling in case of the sample *B*. The phase map was reconstructed at a distance of 156 mm.

The wavefront modifications induced by the micro-lens array onto a collimated laser beam (plane wavefront) were analysed. The phase-map of the transmitted wavefront at the exit pupil of the microlens array can be obtained by the numerical reconstruction of digital holograms, which consists in reconstructing the complex wavefront transmitted by the microlens array by back-propagating the diffraction field. Amplitude and phase maps of the object wavefront can be retrieved from the complex wavefront. Numerical methods and the principle of operation to get wavefront reconstruction are reported in refs. [32] and [42]. Several holograms were recorded at a rate of 1 image per second. The movie in Fig. 6 shows the wrapped phase maps modulus  $2\pi$  corresponding to  $3 \times 4$  lens elements on the incoming collimated beam during the system cool down. The phase curvature indicates the existence of the lens effect. In fact, the curvature of the oil-air interface changes while the sample is cooling, as can be clearly noticed into the movie reported in Fig. 6. This effect could be exploited for having an array of microlenses with variable focus. The number of fringes decreases during the cooling,

indicating that the liquid layer is returning back to its initial condition corresponding to a completely erased waviness and thus to an infinite focal length.

Figure 7 shows a portion of the mod  $2\pi$  unwrapped phase map corresponding to a single frame of the movie in Fig. 6 and allows to estimate the wavefront curvature in correspondence of  $2 \times 2$  micro-lenses of the array.

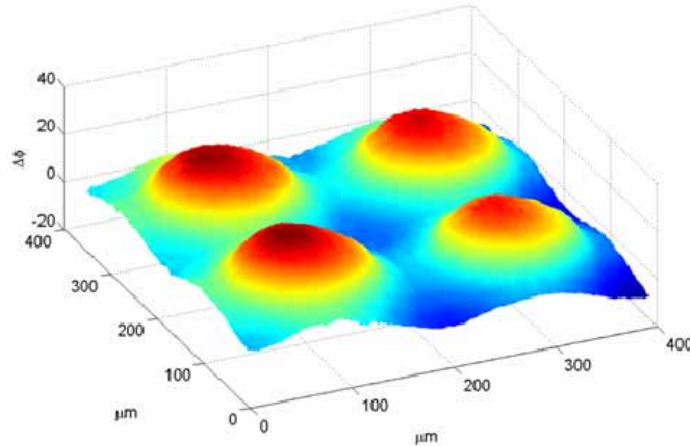


Fig. 7. Unwrapped phase map corresponding to a portion of the image in Fig. 6 for a fixed temperature during cooling.

Fitted parabolic profiles, calculated during cooling, indicate the presence of variable defocus, namely a variable focal length as shown in Fig. 8(a), where the phase profiles of the transmitted wavefront, corresponding to different time frames (1s, 3s, 5s, 7s, 9s, 11s, 13s, 14s) during cooling, are reported. The slight tilt of the sample, respect to the microscope objective into the interferometric set-up, is revealed by the asymmetry of the curves in Fig. 8(a). The focal length  $f$  of the liquid lenses can be retrieved by fitting the unwrapped phase map  $\Phi(x, y)$  to a 2<sup>nd</sup> order polynomial according to

$$\Phi(x, y) = \frac{2\pi}{\lambda} \frac{(x^2 + y^2)}{2f} \quad (3)$$

Figure 8(b) shows the variation of the focal length (from 1.75 mm up to 2.1 mm) corresponding to the time frames of Fig. 8(a) during the cooling process. This effect could be used to have an array of microlenses with variable focus. Moreover, an imaging experiment was also performed in order to show the possibility to use this kind of variable focus microlens array for integrated microscope applications.

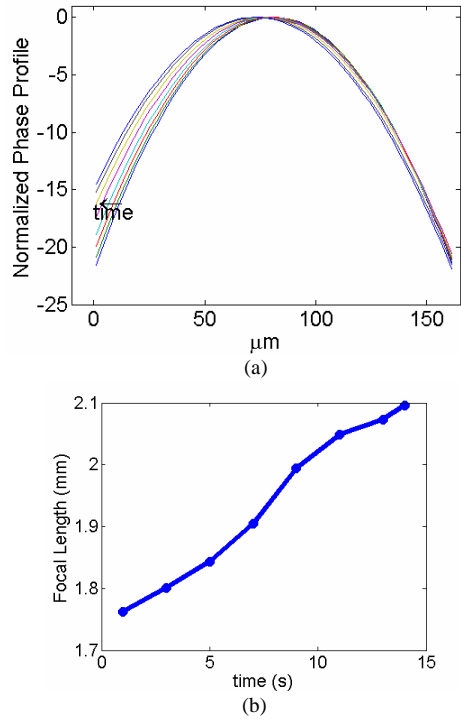


Fig. 8. (a). Phase profiles of the transmitted wavefront calculated for different frames during cooling; (b) focal length values calculated as function of time during the cooling process.

Figure 9 shows the imaging capability of the microlens array on a portion of USAF phototarget. The LN substrate, with the microlens array, was positioned over the target and observed under the optical microscope. The images in Figs. 9(a)-9(b) were acquired at two different focal planes corresponding to focusing the target through the regions outside and inside the aperture of the microlenses, respectively.

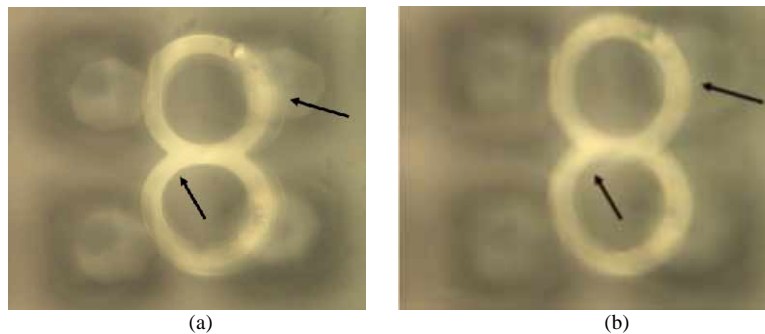


Fig. 9. Optical microscope images of the target “8” observed through the microlens array at two different focal planes imaging the target (a) through the region outside the lenses and (b) through the up-right microlens, where the focusing capability of the microlenses is clearly visible.

Furthermore, different oils with variable densities, such as paraffin oil, primed oil and sweet almond oil, were also used for analogous experiments and the lens effect appeared to work even though exhibiting slight different behaviours depending essentially on the oil density properties.

## 5. Conclusions and further developments

The results presented in this paper show the possibility to build electrowetting devices based on a new concept related to the electrical activation of PPLN substrates by the pyroelectric effect. The configuration is electrodes-less and circuit-less, meaning that the electrodes are “intrinsically embedded” into the material thanks to the micro-engineered LN substrate, thus avoiding the use of heterogeneous materials and processes to change selectively the wettability of the solid surface. Moreover, the material itself is functionalized and can be controlled and activated by temperature variations without any external electric source and physical circuit. For example, temperature variations could be activated remotely and wireless by laser light absorption or by microwaves, just to cite some. Further experiments are being investigated in order to optimize the design and control of the temperature activation, thus providing the possibility to exploit this new configuration in many fields of application within the bio-micro-optofluidics area. For instance, such kind of LN substrates would be part of a PDMS based microfluidic chip (for example squeezed between two PDMS microstructured substrates), allowing to perform flexible imaging of flowing particles, fluids or biological cells, by a relatively simple technique. In fact, the electrode-less configuration would enable higher degree of integration compared to conventional electrowetting devices. The gravity effects and the sealing methods would be similar to those involved in conventional electrowetting-based microfluidic devices fabricated in polydimethylsiloxane (PDMS) and equipped with metal electrodes. Among other developments, a smart microscope slide based on this configuration could be foreseen, such that the surface lenses can be activated by the pyroelectric effect for the microscopic observation in liquid environments. The repeatability of the observed effect after multiple operations was high in the meaning that no differences were observed in various successive cycles. However, a more reliable system for temperature control is under consideration in order to definitively assess the degree of repeatability. Furthermore, the lens alignment issue would be greatly simplified because the microlenses are formed exactly across the hexagonal reversed domains which could be themselves used for preliminary optical alignment. Additional work is in progress to characterize deeper the microlens array even in respect to high aberration orders and imaging properties.

## Acknowledgments

The research leading to these results has received funding from the European Community's Seventh Framework Programme FP7/2007-2013 under grant agreement n° 216105 “Real 3D”. The authors thank Mr. Gregory Genta Jouve for the chemical characterization of the oil sample.